Asymmetry in the Structure of Glycopeptide Antibiotic Dimers: NMR Studies of the Ristocetin A Complex with a Bacterial Cell Wall Analogue

Patrick Groves,† Mark S. Searle, Jonathan P. Waltho,‡ and Dudley H. Williams*

Contribution from the Cambridge Centre for Molecular Recognition, University Chemical Laboratories, University of Cambridge, Lensfield Road, Cambridge CB2 1EW, UK, and Krebs Institute for Biomolecular Research, University of Sheffield, Western Bank, Sheffield S10 2UH, UK

Received February 13, 1995⊗

Abstract: The solution structure of a dimer complex of the glycopeptide antibiotic ristocetin A has been determined from NOE constraints, energy minimization, and molecular dynamics calculations. The structure is that of an asymmetric dimer in which the conformation of the two monomeric units differs in the orientation of the tetrasaccharide attached to the aromatic ring of residue 4. Although hydrogen bonding interactions between the peptide backbones of the two antibiotic monomers occur in a symmetrical head-to-tail orientation, the overall dimer assymmetry arises as a consequence of a parallel, head-to-head alignment of the tetrasaccharides. Thus, in the two monomeric antibiotic conformations that constitute the dimer, the orientations of the tetrasaccharides are related by an ≈180° rotation about the glucose−ring 4 glycosidic bond. The quite different orientation of the tetrasaccharide in each half of the dimer results in significant differences in binding interactions with cell wall peptides occupying the two different sites on the dimer. In one site, the hydrophobic face of glucose interacts with the methyl group of the C-terminal D-alanine of cell wall analogues, while the rhamnose sugar of the same tetrasachharide may act as a hydrophilic "cap" where three hydroxyl groups on the edge of the sugar can mimic a group of water molecules through a network of hydrogen bonds. An arabinose sugar of the other tetrasaccharide occupies a similar position to the rhamnose in the second ligand binding site; its single hydroxyl group may be less effective as a hydrophilic cap, and the hydrophobic interaction to a glucose face (see above) cannot now take place. These observations lead to the conclusion that there may be a marked difference in the ligand binding affinities for the two sites. This conclusion has been confirmed experimentally.

Introduction

Glycopeptide antibiotics have assumed a prominent position in the treatment of Gram-positive bacterial infections.[1] Vancomycin, in clinical use since 1956,[2] is considered the "last line of defence" against methicillin-resistant *Staphylococcus aureus* (MRSA), the often lethal "super-bug".[3] The current high profile of vancomycin and teicoplanin is reflected in yearly sales of these antibiotics that run to hundreds of millions of dollars. Glycopeptide antibiotics, of which several hundred have now been isolated, share a common heptapeptide framework, extensively cross-linked through aromatic side chains, and adorned with various saccharides,[4,5] as illustrated for ristocetin A in Figure 1. The primary mode of action is well-established, involving reversible binding to nascent bacterial cell wall peptides terminating in −D-Ala-D-Ala.[6−9] The proposed hydrogen bonding scheme between the cell wall analogue di-*N*-Ac-L-Lys-D-Ala-D-Ala and ristocetin A is illustrated in Figure 1. The carboxylate binding pocket, consisting of three highly oriented amide NH's (w_2, w_3, and w_4), provides a key feature of cell wall recognition. More recently, the observation that glycopeptide antibiotics form homo-dimers[10−12] has been proposed to add further subtlety and complexity to the molecular basis of antibiotic action.[13] The "back" faces of two antibiotic monomers, not involved in cell wall binding, are able to interact in a head-to-tail arrangement to form a hydrogen bonded dimer (Figure 2A). Moreover, antibiotic activity appears to correlate strongly with the ability to dimerize,[14] rather than directly with binding affinities for cell wall peptides *in vitro*.

Earlier work with eremomycin,[12,13] which carries a disaccharide on ring 4, has shown that the antibiotic dimerizes strongly ($K_{dim} \approx 10^6$ M^{-1}) and that ligand binding and dimerization are cooperative phenomena *in vitro*. Thus, the greater binding affinity of cell wall components for dimer than monomer (factor of ≈ 10) appears to add weight to the proposal that antibiotic dimerization may be intimately involved in the

* Address correspondence to this author at the University of Cambridge.
† Present address: Physical Chemistry 2, University of Lund, Box 124, 22100 Lund, Sweden.
‡ University of Sheffield.
⊗ Abstract published in *Advance ACS Abstracts,* July 1, 1995.

(1) Foldes, M.; Munro, R.; Sorrell, T. C.; Shankar, S.; Toohey, M. *J. Antibiot. Agents Chemother.* **1983**, *11*, 21−26.
(2) McCormick, M. H.; Stark, W. M.; Pittenger, G. E.; Pittenger, R. C.; McGuire, J. M. *Antibiot. Annu.* **1955/6**, 606−611.
(3) Aoki, Y.; Kashiwagi, H. *Chemotherapy (Tokyo)* **1992**, *40*, 997−1004.
(4) Barna, J. C. J.; Williams, D. H. *Annu. Rev. Microbiol.* **1984**, *38*, 339−357.
(5) Nagarajan, R. J. *Antibiot.* **1993**, *46*, 1181−1195.
(6) Nieto, M.; Perkins, H. R. *Biochem. J.* **1971**, *124*, 845−852.
(7) Williams, D. H.; Williamson, M. P.; Butcher, D. W.; Hammond, S. J. *J. Am. Chem. Soc.* **1983**, *105*, 1332−1339.
(8) Williams, D. H.; Waltho, J. In *NMR Spectroscopy in Drug Research, Alfred Benzon Symposium 26*; Munksgaard: Copenhagen, 1988; pp 101−116.
(9) Kannan, R.; Harris, C. M.; Harris, T. M.; Waltho, J. P.; Skelton, N. J.; Williams, D. H. *J. Am. Chem. Soc.* **1988**, *110*, 2946−2953.
(10) Waltho, J. P.; Williams, D. H. *J. Am. Chem. Soc.* **1989**, *111*, 2475−2480.
(11) Gerhard, U.; Mackay, J. P.; Maplestone, R. A.; Williams, D. H. *J. Am. Chem. Soc.* **1993**, *115*, 232−237.
(12) Mackay, J. P.; Gerhard, U.; Beauregard, D. A.; Westwell, M. S.; Searle, M. S.; Williams, D. H. *J. Am. Chem. Soc.* **1994**, *116*, 4581−4590.
(13) Mackay, J. P.; Gerhard, U.; Beauregard, D. A.; Maplestone, R. A.; Williams, D. H. *J. Am. Chem. Soc.* **1994**, *116*, 4573−4580.
(14) Beauregard, D. A.; Williams, D. H.; Gwynn, M. N.; Knowles, D. J. C. *Antimicrob. Agents Chemother.* **1995**, *39*, 781−785.

0002-7863/95/1517-7958$09.00/0

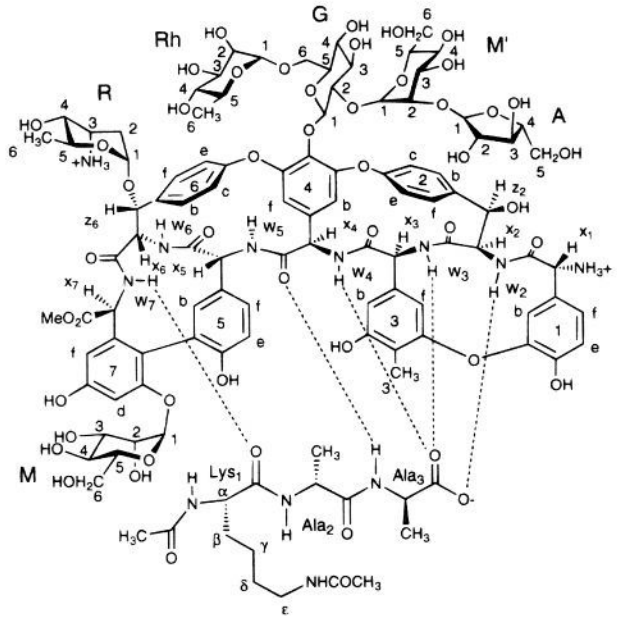

Figure 1. Exploded view of the ristocetin A complex with the cell wall analogue di-*N*-Ac-L-Lys-D-Ala-D-Ala. Hydrogen bonds are indicated by dotted lines; R, ristosamine; Rh, rhamnose; G, glucose; M/M′, mannose; A, arabinose.

mechanism of action *in vivo*.[13] A number of glycopeptides have now been characterized and the thermodynamics of dimerization in the presence and absence of ligands examined.[11-13,15] Ristocetin A represents a unique case in that ligand binding appears to decrease the proportion of dimer present in solution;[13,15] that is, the two molecular recognition events show an apparent "anti-cooperativity". This was an unexpected observation, contrasting with the data for other members of the vancomycin group, potentially invalidating the model proposed for the biological role of dimerization.[13] However, the pseudoaglycon of ristocetin A (ristocetin-Ψ), which lacks the tetrasaccharide and ring 7 mannose, exhibits the positive cooperativity seen for other members of the group,[11] but most importantly, it is a factor of 10 more active than ristocetin A *in vivo* against a range of bacterial strains.[16] This is despite binding di-*N*-Ac-L-Lys-D-Ala-D-Ala ≈10 times less strongly *in vitro* than ristocetin A itself.[17] Thus, the lower antibacterial activity exhibited by ristocetin A (relative to ristocetin-Ψ) appears to be consistent with the "apparent anti-cooperative" relationship between cell wall binding and dimerization.

The role of the tetrasaccharide in the various molecular recognition events remains unclear. Although the tetrasaccharide promotes dimerization in the free antibiotic and enhances ligand binding, its presence appears to lie at the center of the apparent change from the cooperative relationship between ligand binding and dimerization for ristocetin-Ψ to anti-cooperative behavior for ristocetin A. The molecular basis for such a change is investigated here from the determination of the solution structure of the ristocetin A dimer complexed with the cell wall peptide analogue di-*N*-Ac-L-Lys-D-Ala-D-Ala.

Experimental Methods and Materials

Materials. The antibiotic ristocetin A was kindly provided by Abbott Laboratories (Chicago) and Lundbeck (Copenhagen) as the sulfate salt; di-*N*-Ac-L-Lys-D-Ala-D-Ala (di-*N*-Ac-KAA) was purchased from Sigma. A 10 mM sample of ristocetin A in 0.5 mL of 70:30 H_2O:CD_3CN (v/v) was used with 1.0 equiv of tripeptide added. The solution was not buffered but adjusted to pH 7 with NaOD in D_2O solution.

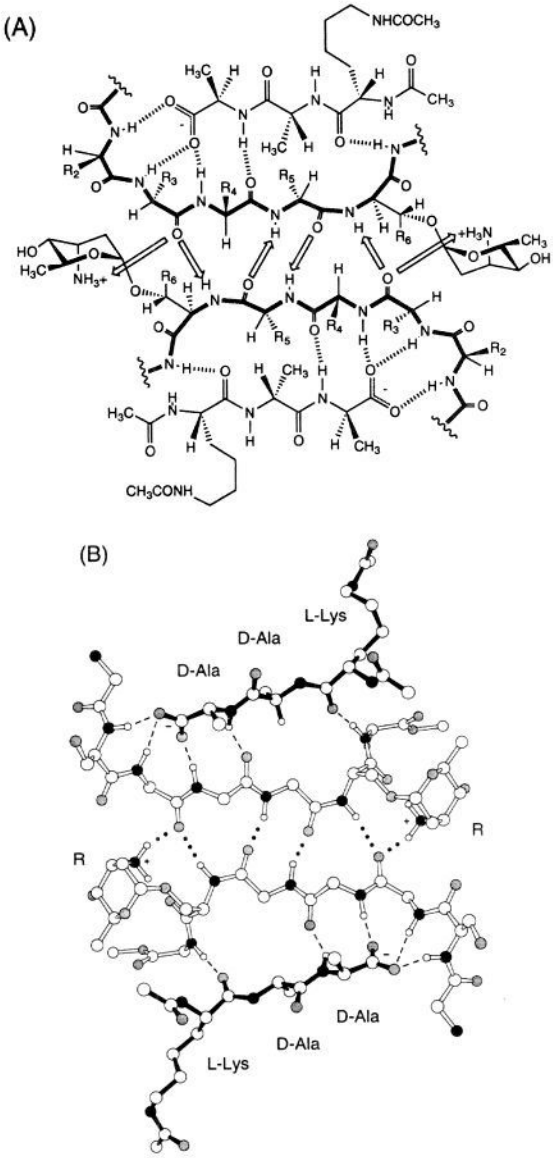

Figure 2. (A) Schematic view of the head-to-tail orientation and hydrogen bonding pattern (arrows) at the dimer interface. Dashed lines represent hydrogen bonds with cell wall components bound to the concave, nondimerizing, faces of the antibiotics. (B) Part of the NOE-restrained, energy-minimized structure of the ristocetin A dimer complex illustrating the same structural features shown schematically in part A, namely, the peptide backbone geometries and hydrogen bonding at the ligand and dimer interfaces. Bound di-*N*-Ac-L-Lys-D-Ala-D-Ala is shown with filled-in bonds. Carbon, open circles; nitrogen, black circles; oxygen, shaded circles.

NMR Spectroscopy. Two-dimensional NMR spectra were recorded on a Bruker AMX500 spectrometer using standard pulse sequences and phase cycling modified with an extended Hahn-echo to improve solvent suppression.[18] The latter was achieved through preirradiation of the water resonance with a 50-Hz field for 1 s. Double quantum filtered scalar correlated spectroscopy (DQF-COSY) experiments were recorded with a t_{1max} of 100 ms and a t_{2max} of 400 ms, with 64 scans per t_1 increment. Total correlated spectroscopy (TOCSY) experiments

(15) Groves, P.; Searle, M. S.; Chicarelli-Robinson, I.; Williams, D. H. *J. Chem. Soc., Perkin Trans. 1* **1994**, 659-665.
(16) Nielsen, R. V.; Hyldig-Nielsen, F.; Jacobsen, K. *J. Antibiot.* **1982**, 1561-1564.
(17) Barna, J. C. J.; Williams, D. H.; Williamson, M. P. *J. Chem. Soc., Chem. Commun.* **1985**, *254*.
(18) Waltho, J. P.; Cavanagh, J. *J. Magn. Reson. Ser. A* **1993**, *103*, 338-348.

were acquired using DIPSI-2 spin-locking of longitudinal magnetization for periods of 50 to 100 ms. Nuclear Overhauser effect spectra (NOESY) were recorded with mixing times of 50, 100, and 200 ms. Both NOESY and TOCSY experiments were acquired with a t_{1max} of 80 ms and t_{2max} of 328 ms, again with 64 scans per increment. Processing of time domain data was performed using the program FELIX (Biosym, San Diego), employing Lorentzian−Gaussian apodization and zero-filling prior to Fourier transformation. Spline-function baseline corrections were subsequently employed in one or both dimensions.

NOE constraints for structure calculations were derived from a single 50-ms NOESY spectrum of the complex. NOEs were calibrated using a number of fixed proton−proton distances within the structure. In general, it was found that NOEs corresponding to protons with a separation of ≥4 Å, which were relatively well-defined by the covalent structure of the antibiotic, had very low intensity in 50-ms NOESY spectra, indicating that ≈4 Å was a reasonable upper limit to interproton distances detected by NOEs at this mixing time. For this reason the upper distance bound used in the NOE restraint file was set to 4 Å while the lower limit was taken as 2 Å representing a value close to the van der Waals contact distance. Thus, all NOEs identified in 50-ms NOESY data were assigned an equal weighting of 3 ± 1 Å reflecting these limits while also allowing for any uncertainties implicit in the two-spin approximation or arising from the effects of internal motions on effective correlation times.

Molecular Modeling. All molecular modeling and structure calculations were performed on a Silicon Graphics Indigo R4000 using MacroModel software.[19] An initial structure of the antibiotic, built within MacroModel, was subjected to conjugate gradient energy minimization, employing AMBER empirical energy functions, to relieve bad contacts between nonbonded atoms and optimize bond lengths and geometries. A dimer structure, with ligands bound, was generated by manually docking the various components while monitoring hydrogen bond lengths. The dimer structures were then subjected to the same energy minimization procedure to remove bad contacts at the dimer interface. A continuum dielectric model appropriate to water was used. The structure was then refined using molecular dynamics calculations. For simulated annealing, initial velocities were assigned to a Maxwell distribution equivalent to 1000 K and the system was allowed to cool to 300 K over a period of 50 ps with 97 intermolecular NOE restraints effective in the form of square-well potentials (force constant of 100 kJ mol^{-1} Å^{-2}). All NOE restraints were assigned an equal weighting of 3 ± 1 Å (see above). All bond lengths were fixed using the SHAKE algorithm.[20] The temperature of the system was then maintained at 300 K by rescaling velocities every 0.2 ps with the time step of the integrator set to 1.5 fs. The total dynamics simulation time was 100 ps with 20 sample structures collected at 5-ps intervals. The last five dynamics structures sampled, all of which fully satisfied the NOE restraints, were refined further using both restrained and unrestrained energy minimization with the final structures again showing no violations of the distance restraints. One of these structures was arbitrarily chosen for illustration in subsequent figures. Coordinates of the ristocetin A dimer complex with di-*N*-Ac-L-Lys-D-Ala-D-Ala are available from the authors on request.

Results

NMR Assignments. Through a combination of high concentration of antibiotic (10 mM) and the addition of 30% CD_3CN to reduce the effects of nonspecific aggregation on NMR line widths, it has been possible to populate almost exclusively (>90%) the dimeric form of the complex, and subsequently assign the majority of resonances in the two halves of the dimer. No significant chemical shift changes were observed on addition of CD_3CN, indicating that this solvent mixture is not inducing any major conformational changes but serves only to reduce the effects of non-specific aggregation leading to a significant improvement in the quality of 2D NMR data. Double quantum filtered correlation spectroscopy (DQF-COSY) and total correlation spectroscopy (TOCSY) were instrumental in identifying spin-coupling pathways, particularly within the sugar spin systems, aromatic side chains, and bound ligands, while strong (short range) nuclear Overhauser effects (NOEs) identified in 50- and 100-ms experiments provide the necessary connectivities between adjacent structural elements on the basis of through-space interactions and provided the many conformational constraints used in structure calculations.

Representative portions of the TOCSY and NOESY spectra of the dimer complex are shown in Figure 3. For example, in the TOCSY spectrum (Figure 3A), the spin systems of each of the sugar residues are partially identified through correlations from the anomeric protons. Two sets of sugars are evident, one set from each non-equivalent half of the dimer. Each half of the dimer is assigned the same proton labels; however, the two halves are distinguished by the use of an asterisk. The spin systems of the two glucose units G and G*, one from each tetrasaccharide, are well resolved since G_1 and G_1* differ in chemical shift by 0.59 ppm. Substantial differences in chemical shift are also observed for Rh_1 and Rh_1*, and A_1 and A_1*. In Figure 3A, additional cross-peaks corresponding to 4b/4f, 4b*/4f*, and x_6/z_6 and x_6*/z_6* are also highlighted.

Structure of the Dimer and Mode of Ligand Binding. A number of intermolecular NOEs between ligand and antibiotic define the orientation of the cell wall analogue within each binding cleft of the dimer; the hydrogen labeling scheme is shown in Figure 1. For example, $Ala_3Me \rightarrow 2e$, $Ala_2Me \rightarrow 1e$, $Ala_3H\alpha \rightarrow 1e/1f$ (Figure 3B), and $Ala_3NH \rightarrow w_4$ are seen in both antibiotic binding pockets and are consistent with the orientation and hydrogen bonding scheme represented in Figure 1.[10] Very small temperature coefficients of between 0.6 and 1.4 ppb K^{-1} are observed for w_2, w_3, w_4, and w_7, further supporting the proposed hydrogen bonding interactions.[21] Our ability to resolve, in large part, two sets of resonances, one set for each component of the dimer, reveals many intermolecular NOEs at the dimer interface. [The two halves of the dimer are distinguished by the use of an asterisk; hence, x → y, or x* → y*, corresponds to intramolecular NOEs, but x → y* is an intermolecular interaction.] For example, NOEs from 6f → 4b*/x_4*, from x_3*/3b* → R_3/R_4, from $R_1 \rightarrow 2c$* and $R_3 \rightarrow 2b$* and the corresponding counterparts from the other half of the dimer (6f* → 4b/x_4, x_3/3b → R_3*/R_4* and from R_1* → 2c and R_3* → 2b), a number of which are highlighted in Figure 3B, clearly establish the head-to-tail orientation of the two monomeric units in the dimer structure (Figure 2). Other key NOEs are highlighted in Figure 3B and are described in the figure legend.

The NOE-restrained energy-minimized structure of the dimer complex (see Methods) showing the peptide backbone interactions at the dimer interface is illustrated in Figure 2B. Antibiotic side chains have been removed for clarity. The hydrogen bonding networks at the dimer interface and between antibiotics and bound ligands are highlighted. The ligand−antibiotic hydrogen bonding interactions have optimal geometries in both sites (Figure 2B), with C=O···HN distances falling in the range 1.79−1.85 Å, representing good van der Waals complementarity between cell wall components and the two antibiotic binding pockets. The lysine side chain, in contrast, appears to be more mobile than the rest of the complex; the observation of ROE cross-peaks, but not NOEs, between protons in the δ and ϵ positions suggests a disordered conformation extended into

(19) Mohamadi, F.; Richards, N. G. J.; Guida, W. C.; Liskamp, R.; Lipton, M.; Caufield, C.; Chang, G.; Hendrickson, T.; Still, W. C. *J. Comput. Chem.* **1990**, *11*, 440−467.

(20) Van Gunsteren, W.; Berendsen, H. J. C. *Angew. Chem.* **1990**, *29*, 992−1023.

(21) Williamson, M. P.; Williams, D. H. *J. Chem. Soc., Perkin Trans. 1* **1985**, 949−956.

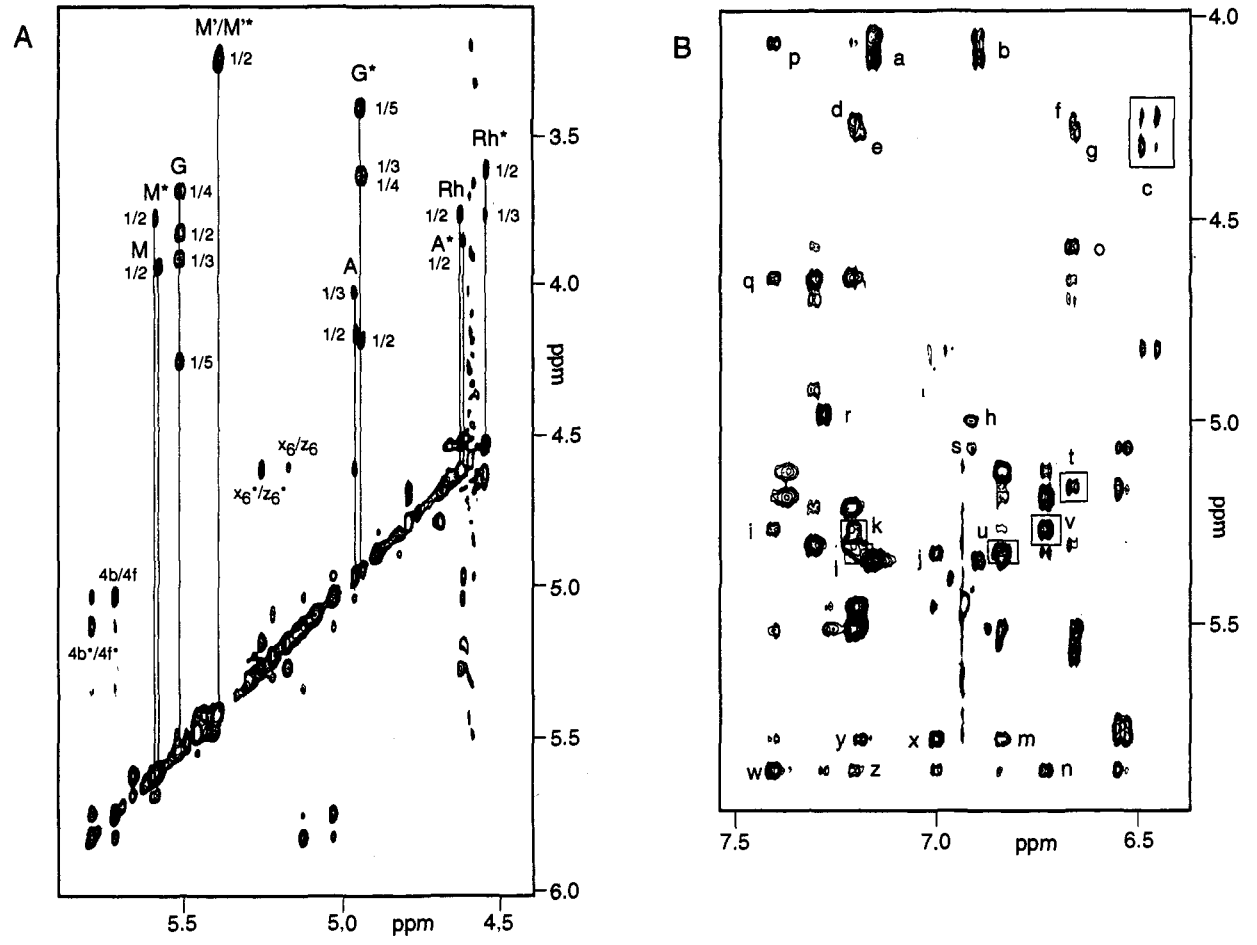

Figure 3. Portions of the 2D TOCSY (A) and 100-ms NOESY spectrum (B) of the dimer complex. In the TOCSY spectrum several correlations within the various sugar spin systems are identified—two sets of resonances are highlighted, one set for each nonequivalent half of the dimer. The sugars of the tetrasaccharides are labeled Rh, G, M′, and A in one half of the dimer (see Figure 1) and Rh*, G*, M′*, and A* in the other half of the asymmetric dimer. The correlations within each sugar originate from the H1 resonance position on the diagonal and are connected by vertical lines. Individual cross-peaks are assigned on the figure, for example, G 1/4 represents a TOCSY correlation for $G_1 \rightarrow G_4$ (see Figure 1). In the portion of the NOESY spectrum shown in part B, a number of key NOEs are highlighted that are relevant to structural features referred to in the text and are labeled as follows: (a) 1f/Ala_3 Hα, (b) 1e/Ala_3 Hα, (c) 7f/Lys_1 Hα are intermolecular NOEs between antibiotic and ligand; (d) R_3/2b*, (e) R_3*/2b, (f) R_3/3b*, and (g) R_3*/3b are intermolecular NOEs between the two halves of the dimer that define the relative backbone geometries and hydrogen bonding patterns involving the ristosamine sugar; (h) 6c/A_1 defines the orientation of one tetrasaccharide over the dimer, while (i) R_1/2c*, (j) R_1*/2c, (k) R_1/2b*, (l) R_1*/2b, (m) 6f*/4b, and (n) 6f/4b* further define the geometry at the dimer interface; (o) 6c*/Rh_1*, (p) 2c*/A_2*, (q) 2c*/A_1*, and (r) 2e*/G_1* define the orientation of the other tetrasaccharide at the dimer interface, while (s) 6c/4f, (t) 6c*/4f*, (u) 6f*/R_1*, (v) 6f/R_1, (w) 4b*/2c*, (x) 4b/2c, (y) 2b/4b, and (z) 2b*/4b* are key NOEs that connect the different residues and are important in assigning the two halves of the dimer.

solution. At the dimer interface the six proposed intermolecular hydrogen bonds have C=O···HN distances between 1,8 and 2,3 Å. The ristosamine amino sugar, attached to the residue 6 side chain, is also illustrated since it also contributes to the hydrogen bonding network. The orientation of this sugar, and hence of the charged amino group, is well determined by many NOEs, in particular $R_3 \rightarrow$ 2b*/3b* and $R_3^* \rightarrow$ 2b/3b, to be ideally positioned to form a hydrogen bond to the carbonyl oxygen of residue 3 of its dimer partner, but also an intramolecular interaction with the carbonyl of residue 6, as shown in Figure 4A. In the structure of the eremomycin dimer,[22] 4-*epi*-vancosamine is attached to the residue 6 side chain; an amino group is similarly attached to the C3 position of the sugar ring, but it is the C3 epimer of the ristosamine sugar in ristocetin A. The positioning of the charged amino group in the equatorial position for eremomycin, but pointing downward in an axial position in ristocetin A, leads to different hydrogen bonding interactions for essentially the same conformation and overall orientation of the sugar. In the eremomycin dimer the amino group hydrogen bonds more effectively to the carbonyl of residue 2 of its dimer partner. The portions of the two structures are illustrated side by side in Figure 4.

We note that the resonances for the NHs of w_5 and w_6, which are proposed to be involved in hydrogen bonding at the dimer interface in the ristocetin A complex, give rise to broad resonances that are partially obscured by overlap with other signals, precluding a detailed examination of their temperature coefficients and exchange rates. However, in the complex of eremomycin, which has a dimerization constant of $\approx 10^8$ M^{-1} in the presence of bound ligand[12] (compared with ≈ 350 M^{-1} for ristocetin A[15]), the NHs w_5 and w_6, which are well resolved, exchange very slowly with solvent such as to persist for many hours after dissolving the antibiotic in D_2O solution. Similarities in the pattern of intermolecular NOEs at the dimer interface for both eremomycin and ristocetin A are consistent with a similar participation of w_5 and w_6 in hydrogen bonding in both dimer complexes.

Dimer-stabilizing interactions are not confined to hydrogen bonds at the interface between the two monomeric units. The cross-linked aromatic side chains of residues 2, 4, and 6 are

(22) Groves, P.; Searle, M. S.; Mackay, J. P.; Williams, D. H. *Structure* **1994**, *2*, 747–754.

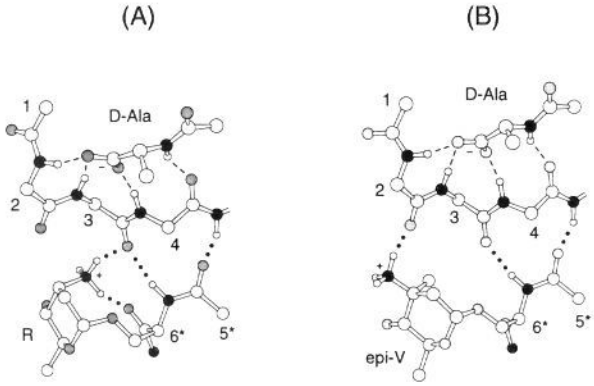

Figure 4. Portions of the dimer complexes of ristocetin A (A) and eremomycin (B) illustrating differences in the hydrogen bonding pattern at the dimer interface involving the different positively charged amino sugars attached to the side chain of residue 6—ristosamine (R), in the case of ristocetin A, and 4-*epi*-vancosamine (*epi*-V), in the case of eremomycin. In each case, the α-carbons of the antibiotic are labeled from the N-terminal residue; residues 1, 2, 3, and 4 are shown (side chains omitted) for one half of the dimer, and residues 5* and 6* for the other half of the dimer. Only the C-terminal fragment of the cell wall peptide (D-Ala) is illustrated.

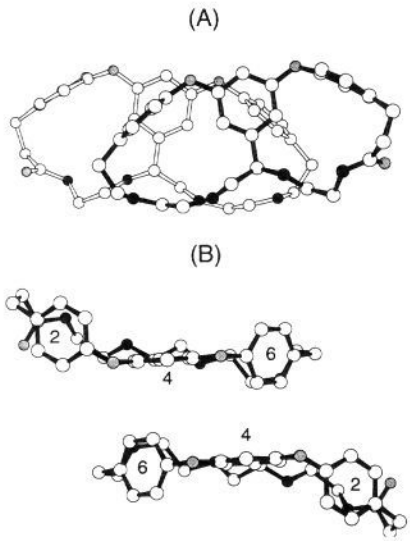

Figure 5. Illustration of edge—face π-interactions at the dimer interface. The antibiotic structures have been stripped down to the peptide backbone and cross-linked aromatic side chains of residues 2, 4, and 6 (labeled in part B). Each half of the dimer is shown (one half filled bonds the other half open bonds). The edge of ring 6 is located against the face of ring 4 of its dimer partner through an off-set, symmetric relationship between the two antibiotic backbones. View from the side (A), view from above (B) [by rotation of (A) by 90°].

conserved in all known glycopeptide structures (with additional chlorine attachments in several cases) and form a relatively rigid template around which all glycopeptide structures are based.[5] Within each monomer, rings 4 and 6 are mutually orthogonal. At the dimer interface, the face of ring 4 and edge of ring 6 of one antibiotic are packed tightly against the edge of ring 6* and face of ring 4* of its dimer partner (Figure 5), such that energetically favorable edge—face π-interactions can contribute to dimer stability.[23] Such a geometry is evident from the large upfield shifts (up to ≈2 ppm) of 6e and 6f that occur on dimerization where these hydrogens are located close to the aromatic face of ring 4.[10] It is evident from the views of the

(23) (a) Hunter, C. A.; Sanders, J. K. M. *J. Am. Chem. Soc.* **1990**, *112*, 5525—5534. (b) Hunter, C. A.; Singh, J.; Thornton, J. M. *J. Mol. Biol.* **1991**, *218*, 837—846.

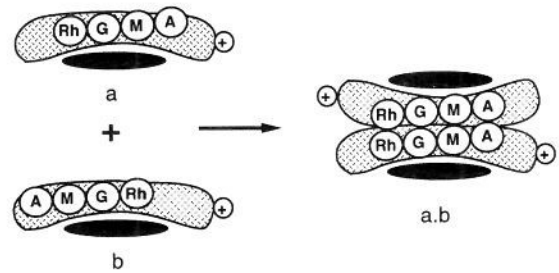

Figure 6. Schematic representation of the two monomeric conformers of the antibiotic **a** and **b** (related by ≈180° rotation of the tetrasaccharide) required to form an asymmetric dimer **a.b**. The hatched region represents the antibiotic (N-terminus indicated by +); tetrasaccharides are represented by the sugar building blocks labeled Rh, G, M, and A (see Figure 1).

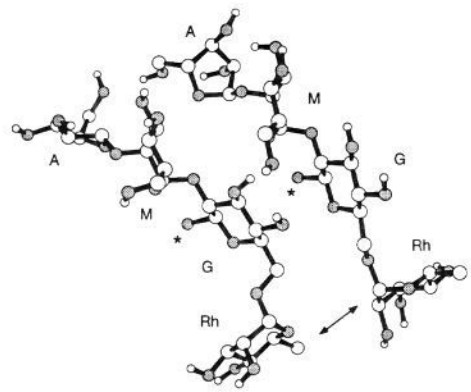

Figure 7. View of the interacting tetrasaccharides in isolation illustrating the parallel head-to-head orientation. The NOE from Rh_6 to R_1* is indicated by an arrow; sugars are labeled as shown in Figure 1. The point of attachment of each glucose sugar to the aromatic side chain of residue 4 is indicated by an asterisk.

structure shown in Figures 2B and 5 that the dimer appears highly symmetrical, yet the NMR spectrum indicates the presence of two independent sets of resonances, one for each half of the dimer, suggesting overall structural asymmetry.

Orientation of the Tetrasaccharides. It is evident from a full analysis of the NOE data that the global asymmetry of the complex arises from the relative orientation of the antibiotic tetrasaccharides that are also involved, through mutual interaction, in dimer stabilization.[11—13] In accord with this conclusion, the largest chemical shift differences between corresponding resonances in the two halves of the dimer occur in the tetrasaccharides and the aromatic portions of residues 2, 4, and 6 that are adjacent to these sugars. A combination of conformations **a** and **b** shown in Figure 6 (related through ≈180° rotations of the tetrasaccharides about the glucose—ring 4 bond) is observed to give rise to the asymmetric dimer structure **a.b**. Structure **a.b** has a parallel alignment of the tetrasaccharides, rather than either of the two possible symmetrical combinations **a.a** or **b.b**, in which the tetrasaccharides are antiparallel. The parallel orientation of the tetrasaccharides in the asymmetric **a.b** dimer is readily apparent from intermolecular NOEs between the tetrasaccharides that are only consistent with this relative orientation. For example, the rhamnose methyl protons (Rh_6) in each half of the dimer experience quite different environments. Rh_6, on the one hand, is found in a hydrophobic pocket defined by the NOEs $Rh_6 \rightarrow R_1$*/z_6*/6b*/Rh_1*. Its counterpart Rh_6*, on the other hand, gives few NOEs (and certainly none that are intermolecular) suggesting solvent exposure of this face of the sugar. Note that the NOEs highlighted above for Rh_6 (particularly $Rh_6 \rightarrow Rh_1$*) are incompatible with either sym-

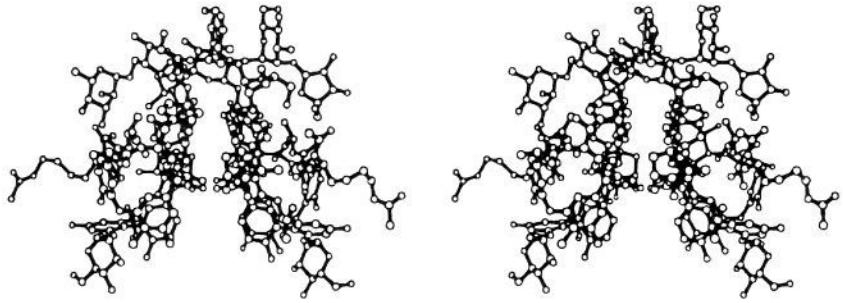

Figure 8. Structure of the ristocetin dimer complex shown as a stereopair. The complex is viewed along the dimer interface.

metrical antiparallel alignment of the tetrasaccharides but compatible with a parallel conformation in which different "faces" of the two tetrasaccharides are brought into contact, as shown in Figure 7. Thus, the NOEs described are uniquely characteristic of an asymmetric dimer. A number of intramolecular NOEs (Rh_1*/Rh_2* → 6c*, A_1 → 6c, and A_1*/A_2* → 2c*; see Figure 3B) are also completely consistent with the proposed conformations. The glycosidic conformations of each of the linked units in each of the tetrasaccharides are also well-defined by strong intramolecular NOEs involving the anomeric protons and those of adjacent sugars (Rh_1 → G_5, M_1 → G_2, A_1 → M_2). Thus, both the conformation and relative orientation of the tetrasaccharides in the dimer complex are well-determined by the NOE data which have been used as input restraints for structure calculations (see Methods).

The parallel alignment of the tetrasaccharides leads to the involvement of different sugars in "capping" the two ligand binding sites, as shown in the stereoview of the dimer complex shown in Figure 8. In one ligand binding pocket (that corresponding to conformation **a** in Figure 6, and the left-hand pocket in Figure 8), hydrophobic contacts are evident between ligand Ala_3Me* and protons on one face of the glucose sugar (G*), consistent with the observation of the NOEs Ala_3Me* → G_1*/G_5*. In the second dimer binding site (conformation **b**), equivalent NOEs are not detected, consistent with ≈180° rotation of the tetrasaccharide which moves the hydrophobic face of the glucose well away from the ligand binding site. The many inter- and intramolecular NOEs place the rhamnose sugar (conformation **a**) and arabinose sugar (conformation **b**) in positions where they could act as hydrophilic "caps" to the ligand binding sites. Again, the extent to which the two sugars might achieve this capping effect is suggested to be different in the two sites. Although we have not assigned specific hydroxyl protons and identified directly through NOEs the hydrogen bonds concerned, the structure calculations, where the orientation of the sugars is restrained by other NOE data, may provide insights into these capping interactions. In conformation **a** (left side of Figure 8), the hydrophilic edge of the rhamnose sugar (namely hydroxyl groups on C3, C4, and C5) is in a position to effectively hydrogen bond to the carbonyl of Ala_2, the NH of Ala_2, and the *N*-acetyl carbonyl of Lys_1, as is evident in the structure of Figure 8 and shown in detail in Figure 9A. The hydroxyls can act as both hydrogen bond donors and acceptors resulting in a network of inter- and intramolecular hydrogen bonds which appear to mimic a group of water molecules that could occupy similar positions when the ligand is present in free solution, but which may be displaced on binding. In the same pocket, the hydrophobic face of glucose effectively occludes the Ala_3 methyl side chain of the cell wall analogue from the solvent (Figure 9A). In contrast, the arabinose, which acts as a hydrophilic cap in conformation **b** (right-hand site in Figure 8), has only a single hydroxyl group that appears to be considerably less effective as a possible

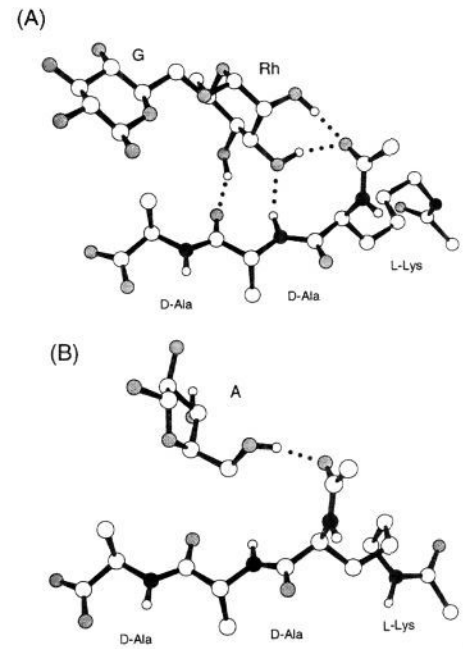

Figure 9. Illustration of the hydrophobic and hydrophilic "capping" interactions in the two ligand binding sites. Only the bound cell wall peptide and the relevant sugars are shown for clarity. In part A, three hydroxyl groups on the edge of the rhamnose sugar (Rh) are in a position to hydrogen bond to NH and carbonyl groups of the cell wall peptide, while the glucose sugar (G) forms a hydrophobic cap that occludes the Ala_3Me group from solvent. In the second binding site (B), an arabinose sugar **A** is located above the ligand binding site. Dotted lines represent hydrogen bonds; atoms are shaded as indicated in Figure 2.

substitute for displaced solvent molecules (Figure 9B). In this binding site the different orientation of the tetrasaccharide with respect to the bound cell wall peptide may result in less effective hydrophobic capping.

These tentative conclusions regarding the role of the tetrasaccharides in mediating ligand binding lead us to suggest that there may be a marked difference in affinity for the two ligand binding sites. This conclusion is supported by experimental data. For example, the complex of the antibiotic monomer with cell wall peptide appears to involve predominantly conformation **a** (Figure 6) in which the rhamnose sugar lies over the ligand binding pocket and the glucose abutts the Ala_3 methyl group. The glucose−ligand interaction corresponding to conformation **a** is evident in the complex of monomeric ristocetin A with di-Ac-KAA in DMSO solvent.[7] If this is also the case in aqueous solution, then the ristocetin A dimer appears to be composed of two monomeric conformers (with quite different orientations of the tetrasaccharides), only one of which appears to be appreciably populated in the momeric complex in solution in the presence of bound ligand. In 1D ^{1}H NMR titration studies

of ristocetin A with di-*N*-Ac-KAA,[13] only one of the two possible D·L species (that is, dimer bound to one ligand) is seen at low ligand to antibiotic ratios, indicating that in the dimer the binding affinities of the two sites also appear to be different. The similarities between the ristocetin A dimer structure and that of eremomycin, previously described,[22] include the parallel, asymmetric arrangement of the ring 4 saccharides. This unusual feature has been confirmed recently in the crystal structure of the ureido-balhimycin dimer,[24] a derivative of an analogue of vancomycin that carries a single glucose on ring 4. In eremomycin, ring 4 carries a disaccharide consisting of a glucose and 4-*epi*-vancosamine. While the glucose sugar of one disaccharide provides an effective hydrophobic "cap" over one cell wall binding site in an analogous manner to that described for ristocetin A, the second binding site of eremomycin, in contrast to ristocetin A, is equally effectively capped by a 4-*epi*-vancosamine. Molecular modeling reveals that very similar nonpolar surface areas are buried in each site, although quite different sugars are used to the same end. Moreover, NMR titration studies in this case strongly suggest that the two binding sites have very similar affinities for cell wall components.[25] The shorter disaccharide of eremomycin is unable to extend far enough along the cell wall binding cleft to provide the hydrophilic capping of the N-terminal lysyl and alanyl residues found for the tetrasaccharides of ristocetin A.

Acknowledgment. We thank the BBSRC, GLAXO, and XENOVA for financial support and the Biomedical NMR Centre, NIMR, Mill Hill, London for access to high-resolution NMR equipment.

Supporting Information Available: Table of chemical shift assignments for the ristocetin A dimer complex with the cell wall peptide analogue di-*N*-Ac-L-Lys-D-Ala-D-Ala and NOE data and table of coordinates for the ristocetin A dimer complex with di-*N*-Ac-L-Lys-D-Ala-D-Ala (12 pages). This material is contained in many libraries on microfiche, immediately follows this article in the microfilm version of the journal, can be ordered from the ACS, and can be downloaded from the Internet; see any current masthead page for ordering information and Internet access instructions.

JA950503I

(24) Sheldrick, G. M.; Paulus, E.; Vertesy, L.; Hahn, F. *Acta Crystallograph. B*, **1995**, *51*, 89–98.

(25) Groves, P. Ph.D. Thesis, University of Cambridge, 1994.